NASA CONTRACTOR REPORT 166516

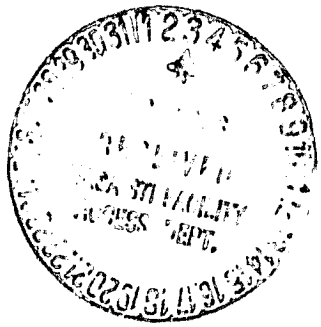

Inlet Free-Stream Turbulence Effects on Diffuser Performance

J. A. Hoffman and G. Gonzales
California Polytechnic State University

CONTRACT NSG-2391
April 1983

NASA

NASA CONTRACTOR REPORT 166516

Inlet Free-Stream Turbulence Effects on Diffuser Performance

J. A. Hoffman and G. Gonzales
Aeronautical and Mechanical Engineering Department
California Polytechnic State University
San Luis Obispo, CA 93407

Prepared for
Ames Research Center
under Grant NSG 2381

National Aeronautics and
Space Administration

Ames Research Center
Moffett Field, California 94035

ABSTRACT

As an extension of a previous study, the performance of a subsonic two-dimensional diffuser was experimentally evaluated as a function of inlet free-stream turbulence parameters. Anisotropic inlet free-stream turbulence with the eddy axis perpendicular to the flow and parallel to the diverging walls of the diffuser appears to be more effective at transmitting energy to the diverging walls of the diffuser, thereby improving diffuser performance, as compared to isotropic turbulence or anisotropic turbulence with the eddy axis perpendicular to the diverging walls of the diffuser. The pressure recovery of the diffuser was found to be strongly dependent upon the inlet free-stream total tubulence intensity, was independent of eddy size for large eddy dimensions, and was dependent upon eddy size for small eddy dimensions. The improvement in the diffuser's static pressure recovery coefficient at a total included divergence angle of 20^{o}, compared to the low inlet turbulence case, was found to be as much as 21 times larger than the pressure loss across the turbulence generators.

NOMENCLATURE

b = distance between parallel walls of diffuser

b_o = rod length

c = channel length

C_p = static pressure recovery coefficient, $(P_2 - P_1)/\rho\bar{U}^2/2$

C_o = pressure loss coefficient across rods, $\Delta P_o/\rho\bar{U}^2/2$

D = rod diameter

H = shape factor of boundary layer at diffuser inlet, δ^*/δ^{**}

L = diffuser wall length

m = slope of R vs. Δs curve

n = number of rods

N = diffuser axial length measured from diffuser inlet

P = static pressure

$\sqrt{\overline{q'^2}}$ = total RMS turbulence component, $\sqrt{(\overline{u'^2} + \overline{v'^2} + \overline{w'^2})/3}$

r = radius of rod set geometry

R_e = Reynolds number, $\bar{U}W'/\nu$

R = free-stream correlation coefficent at diffuser inlet, $\overline{u'(s)\ u'(s - \Delta s)}/\overline{u'^2}$

s = distance in x, y or z direction

$\bar{u}$ = average velocity in flow direction at diffuser inlet

u' = free-stream turbulence component in flow direction at diffuser inlet

$\bar{U}$ = mass average velocity at diffuser inlet

U_m = average free-stream velocity in flow direction at diffuser inlet

v' = free-stream turbulence component in y direction at diffuser inlet

W = diffuser width measured between diverging walls

w' = free-stream turbulence component in z direction at diffuser inlet

δ = boundary layer thickness at diffuser inlet

δ^* = boundary layer displacement thickness at diffuser inlet

δ^{**} = boundary layer momentum thickness at diffuser inlet

θ = divergence angle of diffuser wall

ν = kinematic viscosity

λ = free-stream integral scale of turbulence at diffuser inlet, $\int_0^\infty R\, ds$

ρ = fluid density

ΔC_p = improvement in $C_p(2\theta=20^o)$ compared to no rod case, $C_p(2\theta=20^o) - C_p(2\theta=20^o)_{\text{no rods}}$

Subscripts

0 = location of rods

1 = diffuser inlet ($0.49W_1$ upstream from beginning of diffuser wall curvature)

2 = diffuser exit

x = flow direction

y = direction normal to the flow and parallel to the parallel walls of the diffuser

z = direction normal to the flow and perpendicular to the parallel walls of the diffuser

TABLE OF CONTENTS

LIST OF FIGURES

INTRODUCTION

Many previous investigators (1, 2, 3, 4 and 5) have observed that increases in diffuser performance occurred when the inlet flow was disturbed. Hoffmann (6, 7) has recently correlated increases in diffuser performance with the following free-stream turbulence parameters measured at the inlet to the diffuser: (1) the dimensionless integral scale of turbulence in the flow direction (λ_x/δ^*), (2) the total turbulence intensity ($\sqrt{q'^2}/U_m$), and (3) the orientation of the predominant eddy axis. It is the purpose of the present study to review the experimental procedure used by Hoffmann (6, 7), and to present results obtained using improved experimental techniques. Correlations between diffuser performance and turbulence parameters are presented, and the improvement in diffuser performance is compared to the energy loss of the turbulence generators.

EXPERIMENTAL SYSTEM AND PROCEDURE

The inlet, channel and diffuser used in this investigation are shown in Figure 1. Upstream rods used for turbulence generation are illustrated in Figure 2a; the axes of rod sets GH, JH and KH are parallel to the y axis, while the axes of all the other rod sets are parallel to the z axes. Rod set O (Figure 2b) has rods parallel to the z axis which are positioned flush against the inlet of the channel; the solidity of rod set O is 0.50. Geometrical information about each rod set is presented in Table 1, and dimensions of the experimental system are presented in Table 2.

All velocity and turbulence measurements were obtained using hot wire anemometers and other instrumentation described by Hoffmann (7). All data were obtained with an inlet Reynolds number of 7.83×10^4. Values of the dimensionless boundary layer displacement thickness and the shape factor of the turbulent boundary layer at the diffuser inlet (Section 1 in Figure 1) are presented in Table 2.

Numerous problems were encountered in obtaining pressure recovery and hot wire turbulence measurements during the initial phase of the project. Techniques used and problems encountered are described below.

1. Wire Sensing Length

Initial unpublished measurements were obtained using standard TSI Model 1210 single wire probes and standard Model 1241 X-probes, with 0.00015 in. (0.004 mm) diameter tungsten wires with 0.05 in. (1.3 mm) sensing lengths. The X-wire traverses in the free-stream incorrectly indicated that $\sqrt{\overline{u'^2}}$ and

$\sqrt{\overline{v'^2}}$ were functions of y, and the minimum free-stream value of $\sqrt{\overline{u'^2}}$ indicated by the X-wire probe was approximately 25% larger than that indicated by the single wire. Also, for the same free-stream velocity, the average voltage output of each wire of the X-probe wires changed for different rod sets. It is believed that a spacial resolution problem and/or a probe interference problem existed.

The results presented by Hoffmann (6, 7) were obtained using 0.02in. (0.5 mm) sensing length wires, and the spacing between the wires of the X-probe was modified to 0.005in. (0.13 mm). The results for $\sqrt{\overline{u'^2}}$ obtained with the single wire and the X-probe agreed; these results were approximately 25% larger than those obtained with the 0.05in. length single wire. The indicated free-stream turbulence intensities were independent of y.

2. Frequency Response

When standard TSI Model 10110-15 ft. low resistance cables were used between the probes and the anemometers, the frequency response of the hot wire, obtained using the method of Freymuth (8), was approximately 40,000 Hz. This frequency response increased to about 50,000 Hz when 6 ft. cables were used, and increased to about 60,000 Hz with the use of 3 ft. cables. The results presented by Hoffmann (6, 7) were obtained using a frequency response of about 40,000 Hz, while those of this study were obtained using a frequency response of about 60,000 Hz. The anemometer's response to a square wave showed a significant undershoot after the main pulse unless the bridge was operated off-balance with a high standby voltage, as recommended by Borgos (9). The low pass filter built into the anemometer (-2 db at 100,000 Hz) along with external high pass filters (-3 db at 0.3 Hz) were used with all hot

wire measurements. Meier (10) has shown that small differences in λ_x and $\sqrt{\overline{u'^2}}/U_m$ occur when using different high pass filters (2 Hz to 10 Hz) when $\sqrt{\overline{u'^2}}/U_m$ was 1%, but found significant differences in measured values of λ_x and little difference in $\sqrt{\overline{u'^2}}$ when $\sqrt{\overline{u'^2}}/U_m$ was 0.2%.

3. Conditions of the Hot Wire

The turbulence measurements obtained using limp and/or dirty wires were different than those obtained from taut, clean wires. Dirt buildup occurred on the hot wires; wires were cleaned after every several hours of use by immersion for a two-second period in a rubbing alcohol bath in an ultrasonic cleaner. A new or clean wire appears shiny when observed under a microscope; care was taken in this study to use clean, taut wires.

4. Unsteady Flow

In early measurements (unpublished results), poor flow conditions into the fan caused low frequency flow oscillations; correspondingly, the correlation coefficients at the channel exit remained positive at large time delays. Also, a cotton cloth draped between the topplate and baseplate upstream of the rods, which served to dampen room air currents and to filter the air, initially had folds at two locations. The free-stream longitudinal turbulence intensity for the condition of no upstream rods was reduced from 1% to 0.5% by elimination of the folds.

5. Pressure Recovery Measurements

A smooth transition from the channel to the diffuser (e.g., the diffuser's lid must be flush with the inlet channel) is required in order to

obtain good diffuser performance. Also, electronic time averaging of the pressure ratio $(P_2 - P_1)/(P_0 - P_1)$ should be used to reduce the uncertainty of the C_p measurements reported by Hoffmann (6, 7).

6. Techniques for Obtaining Correlation Coefficients and Integral Scales of Turbulence

All correlation coefficients were obtained with a TSI 1015A correlator using the method suggested by TSI. Values of R_x and λ_x were obtained using TSI Model 1210 single wire probes, with the associated instrumentation and method described by Hoffmann (7). Correlation coefficients in the y and z directions were obtained using two TSI Model 1244 probes; each probe has two parallel wires in the y-z plane with distance between the wires (Δs) of 0.038 in. (0.95 mm) and 0.083 in. (2.12 mm). The correlation coefficients in the y and z directions of each rod set fit exponential equations of the form $R = e^{-m\Delta s}$, as shown in Figure 3. Values of m were obtained from the plots of R vs $\Delta s/\delta^*$ on semi-log paper, and mathematical integration was used to obtain the integral scales of turbulence.

RESULTS AND DISCUSSION

Using improved measurement techniques, the free-stream total turbulence intensity, $\sqrt{q'^2}/U_m$, and the free-stream integral scale of turbulence in the flow direction at the diffuser inlet (section 1), λ_x, were obtained and are compared with previously reported results (6); also, the free-stream integral scales of turbulence in the y and z directions at the diffuser inlet, λ_y and λ_z, were obtained. Correlations between the static pressure recovery coefficient of the diffuser, C_p, the total turbulence intensity, the integral scale of turbulence in the flow direction, an average free-stream eddy size parameter, $(\lambda_x + \lambda_y + \lambda_z)/3\delta^*$, and a free-stream eddy volume parameter, $(\lambda_x\lambda_y\lambda_z)/\delta^{*3}$, are made. Also, the pressure loss coefficient of the rods is presented and compared to the improvement in the static pressure recovery coefficient of the diffuser.

New measurements of $\sqrt{q'^2}/U_m$ are presented in Table 1; these results are an average of 3.7% larger than the results presented by Hoffmann (6). Plots of $C_p(2\theta = 12^o)$ vs. $\sqrt{q'^2}/U_m$ and $C_p(2\theta = 20^o)$ vs. $\sqrt{q'^2}/U_m$ presented in Figures 4 and 5 indicate that $\sqrt{q'^2}/U_m$ and eddy axis orientation are two very important parameters affecting diffuser performance. The largest values of C_p ($C_p(2\theta = 12^o) \geq 0.785$ and $C_p(2\theta = 20^o) \geq 0.701$) which occur for rod sets with axes in the z direction (and corresponding predominant eddy axis in the z direction) were obtained when $\sqrt{q'^2}/U_m > 3.5\%$. These conclusions are the same as those presented by Hoffmann (6). However, rod sets E and O, rod sets with axes in the z direction, do not fit the contours of C_p vs. $\sqrt{q'^2}/U_m$ in Figures 4 and 5. Both rod sets have values of $\sqrt{q'^2}/U_m \geq 4.96\%$ but low values of C_p ($C_p(2\theta=12^o) \leq$

0.771 and $C_p(2\theta=20^o) \leq 0.675$). Rod set O is unique compared to all other rod sets; the turbulence is close to isotropic. For rod set O, $\sqrt{v'^2}/\sqrt{u'^2}=1.07$ and $\sqrt{w'^2}/\sqrt{v'^2}=0.83$, while for all other rod sets evaluated (excluding the no rod case), $\sqrt{v'^2}/\sqrt{u'^2} \geq 1.62$ and $0.62 \leq \sqrt{w'^2}/\sqrt{v'^2} \leq 0.75$. For all rod sets with high values of C_p ($C_p(2\theta=12^o) \geq 0.785$ and $C_p(2\theta=20^o) \geq 0.701$) the turbulence is highly anisotropic ($\sqrt{v'^2}/\sqrt{u'^2} \geq 2.01$ and $\sqrt{w'^2}/\sqrt{v'^2} \leq 0.69$); the turbulence of rod set E is more isotropic ($\sqrt{v'^2}/\sqrt{u'^2} = 1.71$). The low values of C_p obtained with high values of $\sqrt{q'^2}/U_m$ ($\sqrt{q'^2}/U_m \geq 5.78\%$) for rod sets GH and JH has been ascribed to the eddy axis orientation for these rod sets (6). As a result of a near isotropic turbulence, a predominant eddy axis orientation may not exist for rod set O. It appears that if a highly anisotropic turbulence ($\sqrt{v'^2}/\sqrt{u'^2} > 1.71$) with a predominant eddy axis orientation in the z direction does not exist, larger values of $\sqrt{q'^2}/U_m$ may be required to obtain large values of C_p. For rod sets with axes in the y direction, a $\sqrt{q'^2}/U_m = 7.4\%$ (for rod set KH) was required to obtain relatively large values of C_p ($C_p(2\theta=12^o)=0.773$ and $C_p(2\theta=20^o)=0.699$). The results suggest that other parameters (eg. vorticity around the z axis measured at, for example, $y=\delta$, and anisotropy ratios) may correlate well with C_p.

Measurements of free-stream values of λ_x, λ_y, and λ_z at the diffuser inlet were obtained and are presented in Table 1. The values of λ_x/δ^* are an average of 22% lower compared to those presented by Hoffmann (6); the lower values of λ_x/δ^* are believed to be primarily due to the use of clean hot wires and improved frequency response. The results show that $\lambda_y \sim \lambda_z$ and $1.5 < \lambda_x/\lambda_y < 3.4$.

In order to investigate possible correlations between Cp, $\sqrt{q'^2}$, $\lambda x/\delta^*$,

$(\lambda_x + \lambda_y + \lambda_z)/3\delta^*$ and $(\lambda_x\lambda_y\lambda_z)/\delta^{*3}$, the graphs shown in Figures 6, 7 and 8 were constructed. Contours were drawn ignoring data for rod sets with axes in the y direction and data for rod sets E and O, rod sets which produce relatively weak anisotropic inlet turbulence ($\sqrt{\overline{v'^2}}/\sqrt{\overline{u'^2}} \leq 1.71$) and relatively high inlet total turbulence intensities ($\sqrt{\overline{q'^2}}/U_m > 3.5\%$). These plots indicate that the largest values of C_p, ($C_p(2\theta = 12^o) \geq 0.785$ and $C_p(2\theta = 20^o) \geq 0.701$) occur when the following conditions exist.

1) For relatively large eddy size parameters ($\lambda_x/\delta^* > 5$, $(\lambda_x + \lambda_y + \lambda_z)/3\delta^* > 4$ or $(\lambda_x\lambda_y\lambda_z)/\delta^{*3} > 60$), C_p is independent of eddy size, and the largest values of C_p are obtained when $\sqrt{\overline{q'^2}}/U_m > 3.5\%$.

2) For relatively small eddy size parameters ($\lambda_x/\delta^* < 5$, $(\lambda_x + \lambda_y + \lambda_z)/3\delta^* < 4$ or $(\lambda_x\lambda_y\lambda_z)/\delta^{*3} < 60$), C_p is a function of both $\sqrt{\overline{q'^2}}/U_m$ and the eddy size parameters; to obtain the largest values of C_p, larger values of $\sqrt{\overline{q'^2}}/U_m$ are required as the eddy size parameters became smaller.

A tabulation of the ratio of the increase in C_p ($2\theta = 20^o$) compared to the no rod case, to the pressure loss coefficient of the rods, $\Delta C_p/C_o$, is presented in Table 1. The results show that the increases in the static pressure rise of the diffuser at $2\theta = 20^o$ is less than the pressure loss across the rods for rod sets A and O ($\Delta C_p/C_o < 1$), but is larger for all other rod sets. For rod sets G and J, the improvement in the static pressure rise of the diffuser at $2\theta = 20^o$ is 21 times larger than the pressure loss across the rods.

The estimated uncertainty due to random errors of the values of C_p, $\sqrt{\overline{q'^2}}/U_m$, λ_x/δ^*, λ_y/δ^*, and λ_z/δ^*, obtained using the method of Kline and McClintock (11) with 20:1 odds, are presented in Table 3.

CONCLUSIONS

An experimental evaluation of the effects of inlet free-stream turbulence on the performance of a subsonic two-dimensional diffuser has been made. At the inlet of the diffuser, the free-stream turbulence has eddy length dimensions on the order of the thickness of the turbulent boundary layers. The static pressure recovery coefficient of the diffuser at a total included divergence angle of 20° was increased more than 21% with inlet turbulence. This increase in C_p was obtained with anisotropic inlet free-stream turbulence ($\sqrt{\overline{v'^2}}/\sqrt{\overline{u'^2}} > 2$ and $\sqrt{\overline{w'^2}}/\sqrt{\overline{v'^2}} < 0.7$), with the eddy axis perpendicular to the flow and parallel to the diverging walls of the diffuser, and with high values of inlet free-stream total turbulence intensity ($\sqrt{\overline{q'^2}}/U_m > 3.5\%$). Within the range of eddy dimension obtained, diffuser performance appears to be a function of eddy size for small eddy dimensions ($\lambda_x/\delta^* < 5$, $(\lambda_x + \lambda_y + \lambda_z)/3\delta^* < 4$ or $(\lambda_x \lambda_y \lambda_z)/\delta^{*3} < 60$) and appears independent of eddy size for larger eddy dimensions. Although it may be dangerous to draw firm conclusions from limited data, the results suggest that isotropic free-stream turbulence (with no dominant eddy axis orientation) or free-stream turbulence with the eddy axis perpendicular to the diverging walls of the diffuser is less effective at transmitting energy to the diverging walls of the diffuser (larger values of $\sqrt{\overline{q'^2}}/U_m$ may be required to obtain large values of C_p). A $\sqrt{\overline{q'^2}}/U_m = 7.4\%$ was required to obtain high values of C_p when the free-stream eddy axis was perpendicular to the diverging walls of the diffuser. Research remains to be done to precisely define these effects.

The ratio of the increase in the static pressure recovery of the diffuser

at a total included divergence angle of 20° (compared to the case of no upstream rods) to the pressure loss across the rods was as high as 21 for two rod sets.

The turbulence intensity measurements from this study agree well with those from a previous study (6); the free-stream integral scales of turbulence in the flow direction were an average of 22% lower compared to those of the previous study, a result of improved measurement techniques.

ACKNOWLEDGEMENT

The authors gratefully acknowlege the support of this investigation by NASA-ARC through Grant NSG-2391, and the work of student assistants Dean Miller and Mark Thut.

BIBLIOGRAPHY

1. Stevens, S.J. and Williams, G.J., "The Influence of Inlet Conditions on the Performance of Annular Diffusers," ASME Journal of Fluids Engineering, Sept. 1980, pp. 357-363.

2. Viets, H., Ball, M. and Bougine, D. "Performance of Forced Unsteady Diffusers," AIAA Paper 81-0154, presented at the 19th Aerospace Science Meeting, Jan. 12-15, 1981, St. Louis, Missouri.

3. Moore, C.A., Jr. and Kline, S.J., "Some Effects of Vanes and of Turbulence on Two-Dimensional Wide Angle Subsonic Diffusers," Department of Mechanical Engineering, Stanford University, Sept. 1, 1955.

4. Waitman, B.A., Reneau, L.B. and Kline, S.J., "Effects of Inlet Conditions on Performance of Two-Dimensional Diffusers," Journal of Basic Engineering, Trans. ASME, Series D, Vol. 83, 1961, pp. 349-360.

5. Sajben, M., Chen, C.P. and Kroutel, J.C., "A New Passive Boundary Layer Control Device," Journal of Aircraft, Vol. 14, No. 7, July 1977, pp. 654-660.

6. Hoffmann, J.A., "Effects of Free-Stream Turbulence on Diffuser Performance," ASME Journal of Fluids Engineering, Vol. 103, Sept. 1981, pp. 385-390.

7. Hoffmann, Jon A., "Effects of Free-Stream Turbulence on Diffuser Performance," NASA-CR-163194, June 1980.

8. Freymuth, Peter, "Feedback Control Theory for Constant Temperature Hot Wire Anemometers," The Review of Scientific Instruments, Vol. 38, No. 5, May 1967, pp. 677-681.

9. Borgos, J.A., "A Review of Eletrical Testing of Hot-Wire and Hot-Film Anemometers," TSI Quarterly, August/September, 1980.

10. Meier, H.U. and Kreplin, H.P., "Influence of Free-Stream Turbulence on Boundary-Layer Development," AIAA Journal, Vol. 18, No. 1, Jan. 1980, pp. 11-15.

11. Kline, S.J. and McClintock, F.A., "Describing Uncertainties in Single Sample Experiments," Mechanical Engineering, Jan. 1953, pp. 3-8.

TABLE 1

Summary of Results

Rod Set	D/W_1	r/W_1	n	C_o(%)	$C_p(2\theta=12^o)$	$C_p(2\theta=20^o)$	$\Delta C_p/C_o$	$\sqrt{q'^2}/U_m$(%)	$\sqrt{v'^2}/\sqrt{u'^2}$	$\sqrt{w'^2}/\sqrt{v'^2}$	λ_x/δ^*	λ_y/δ^*	λ_z/δ^*
None	-	-	0	0.1	0.705	0.577	0	0.48	1.04	0.86	-	-	-
A	0.18	2.93	19	1.7	0.716	0.589	0.7	2.54	1.71	0.74	3.4	2.2	2.1
B	0.18	4.39	35	0.8	0.710	0.595	2.3	2.50	2.29	0.70	4.6	2.4	2.5
C	0.37	2.93	11	2.5	0.753	0.660	3.3	2.99	1.62	0.73	3.4	2.3	2.2
D	0.37	3.90	11	0 8	0.729	0.625	5.0	2.58	1.99	0.75	4.3	2.4	2.3
E	1.28	2.93	3	2.4	0.771	0.675	4.1	4.96	1.71	0.68	6.0	3.1	3.3
F	1.28	4.39	5	0.9	0.796	0.701	14	3.68	2.08	0.69	4.1	2.5	2.8
G	1.28	5.85	7	0.5	0.777	0.683	21	2.74	2.79	0.68	7.4	2.9	2.7
GH	1.28	5.85	7	1.5	0.751	0.649	4.8	5.78	2.66	0.71	7.9	-	-
H	1.28	5.51	7	0.6	0.773	0.679	17	2.92	2.47	0.71	5.9	2.6	2.8
I	4.39	8.78	3	0.3	0.752	0.612	12	2.46	3.83	0.63	11.0	3.2	3 2
J	4.39	7.80	3	0.5	0.779	0.683	21	2.92	3.08	0.65	9.1	3.1	3.1
JH	4.39	7.80	3	1.5	0.754	0.686	7.3	6.23	2.96	0.69	8.5	-	-
K	4.39	9.76	5	1.1	0.792	0.712	12	4.97	3.03	0.64	6.7	3.3	3.9
KH	4.39	9.76	5	2.3	0.773	0.699	5.3	7.40	2.85	0.67	8.3	-	-
L	4.39	6.83	3	1.1	0.792	0.702	11	4.78	2.42	0.62	7.3	3.0	3.7
M	1.83	3.73	3	1.7	0.785	0.717	8.2	5.33	2.01	0.64	5.9	3.0	3.2
N	2.99	7.32	5	0.7	0.788	0.715	20	3.82	2.53	0.66	5.3	3.2	3.0
O	0.18	-	9	15.0	0.722	0.630	0.35	5.01	1.07	0.83	6.2	-	-

TABLE 2

Dimensions of Experimental System

W_1 = 1.024 in. (2.60 cm)

L/W_1 = 14.7

b/W_1 = 5.86

c/W_1 = 4.88

b_o/b = 1.71

Inlet Boundary Layer Parameters

Rod Sets GH, JH, KH	Other Rod Sets
$2\delta^*/W_1$ = 0.034	$2\delta^*/W_1$ = 0.040
H = 1.56	H = 1.56

TABLE 3

Estimated Uncertainties

Quantity	Rod Sets	Uncertainty (20:1 odds)
C_p	all	± 5%
$\sqrt{\overline{q'^2}}/U_m$	A through H	± 7%
	None and I through O	± 14%
λ_x/δ^*,	A through D	± 10%
λ_y/δ^* and	E through O	± 15%
λ_z/δ^*		

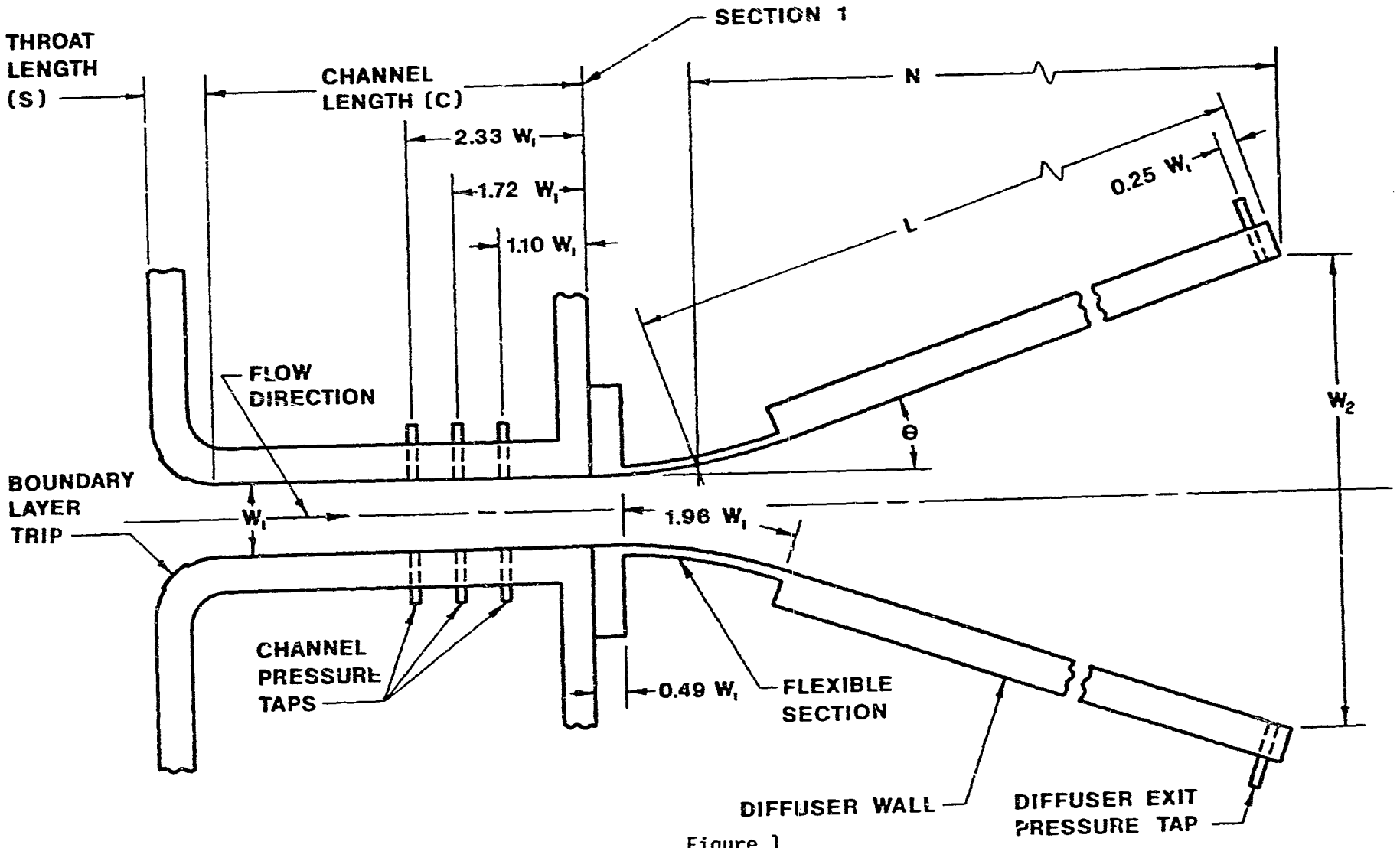

Figure 1

Inlet, Channel, and Diffuser

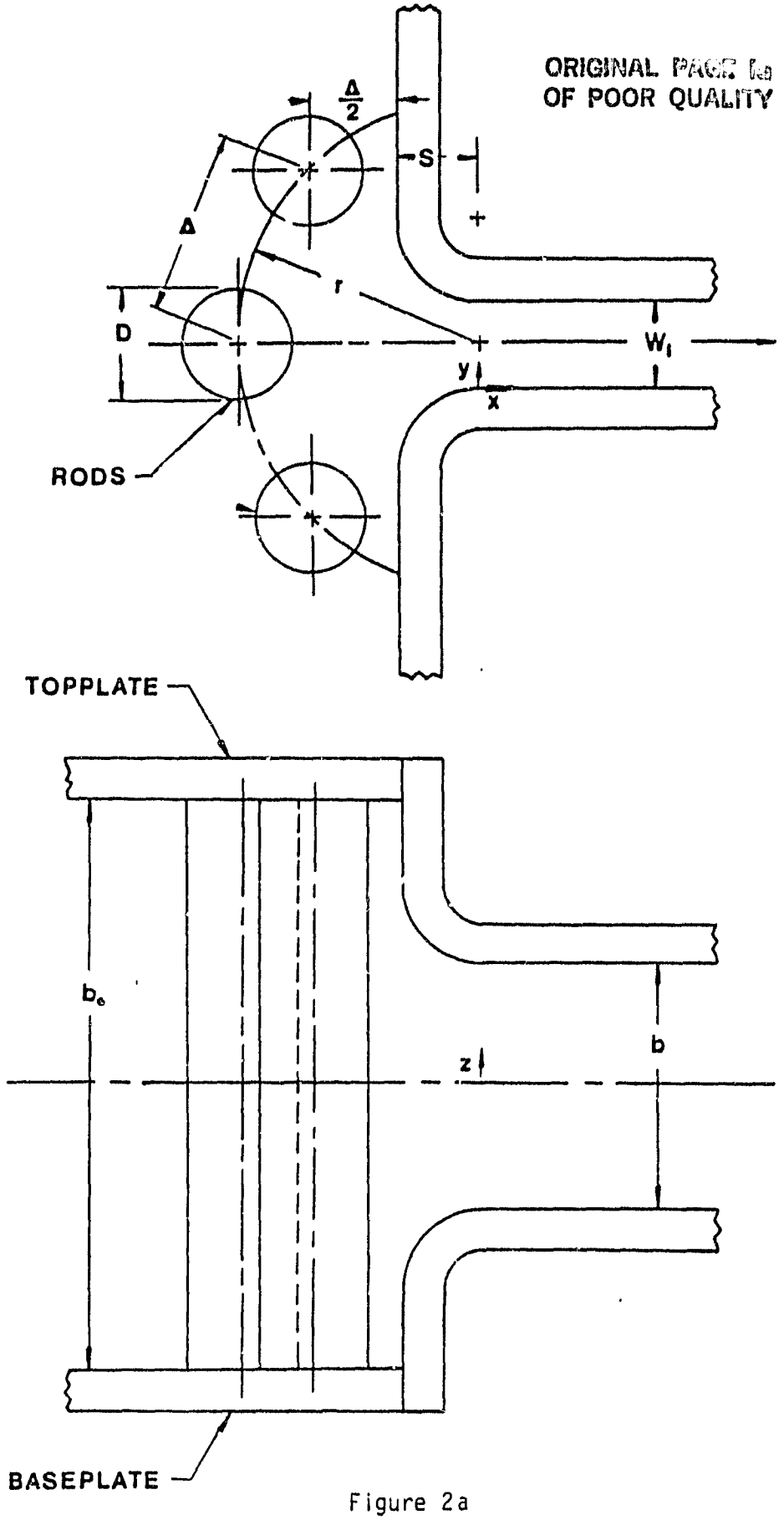

Figure 2a

Rod Set Geometry Nomenclature

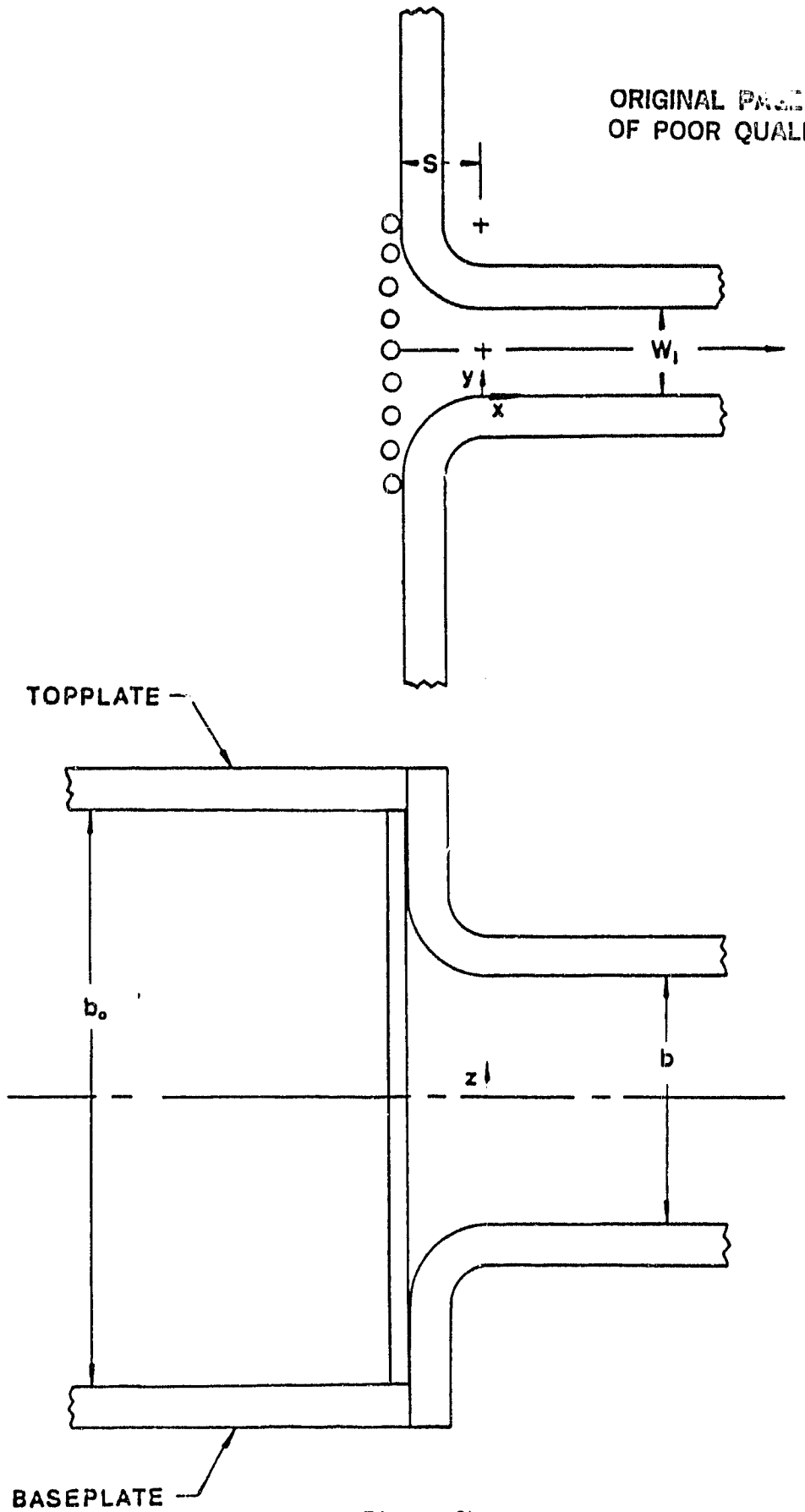

Figure 2b

Rod Set 0

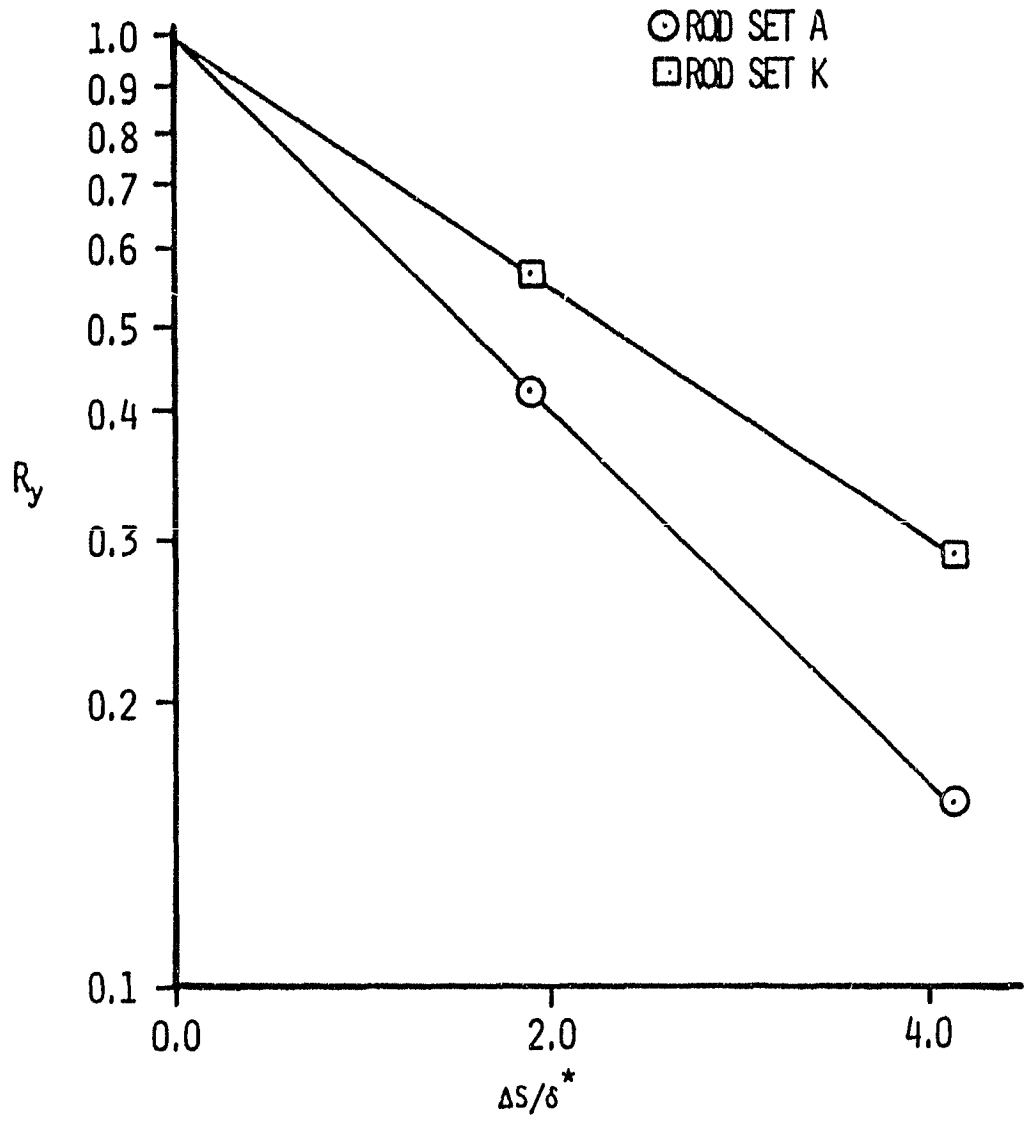

Figure 3
R_y vs. $\Delta S/\delta^*$ for Rod Sets A and K

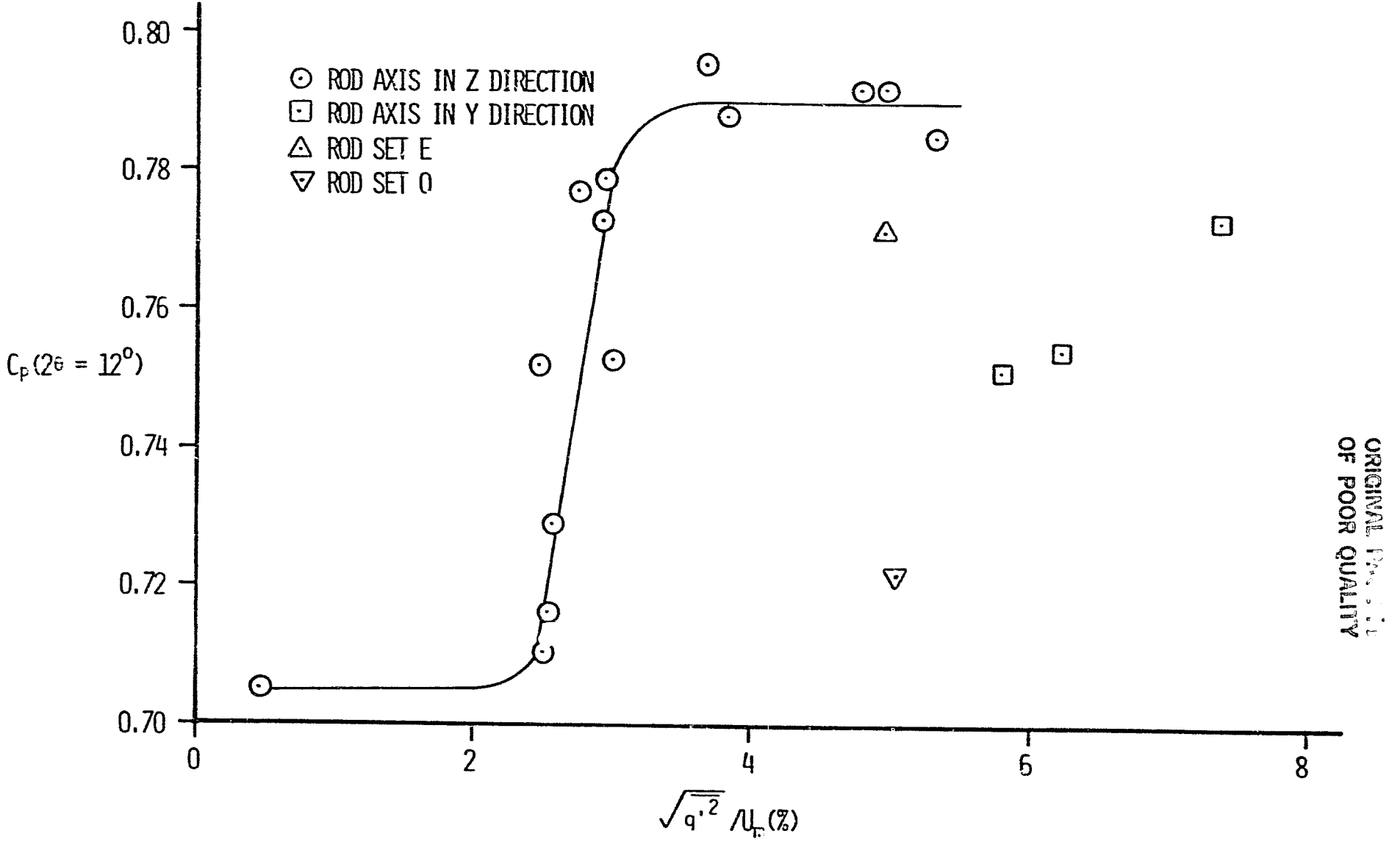

Figure 4

$C_p(2\theta = 12^o)$ vs. $\sqrt{q'^2}/U_m$

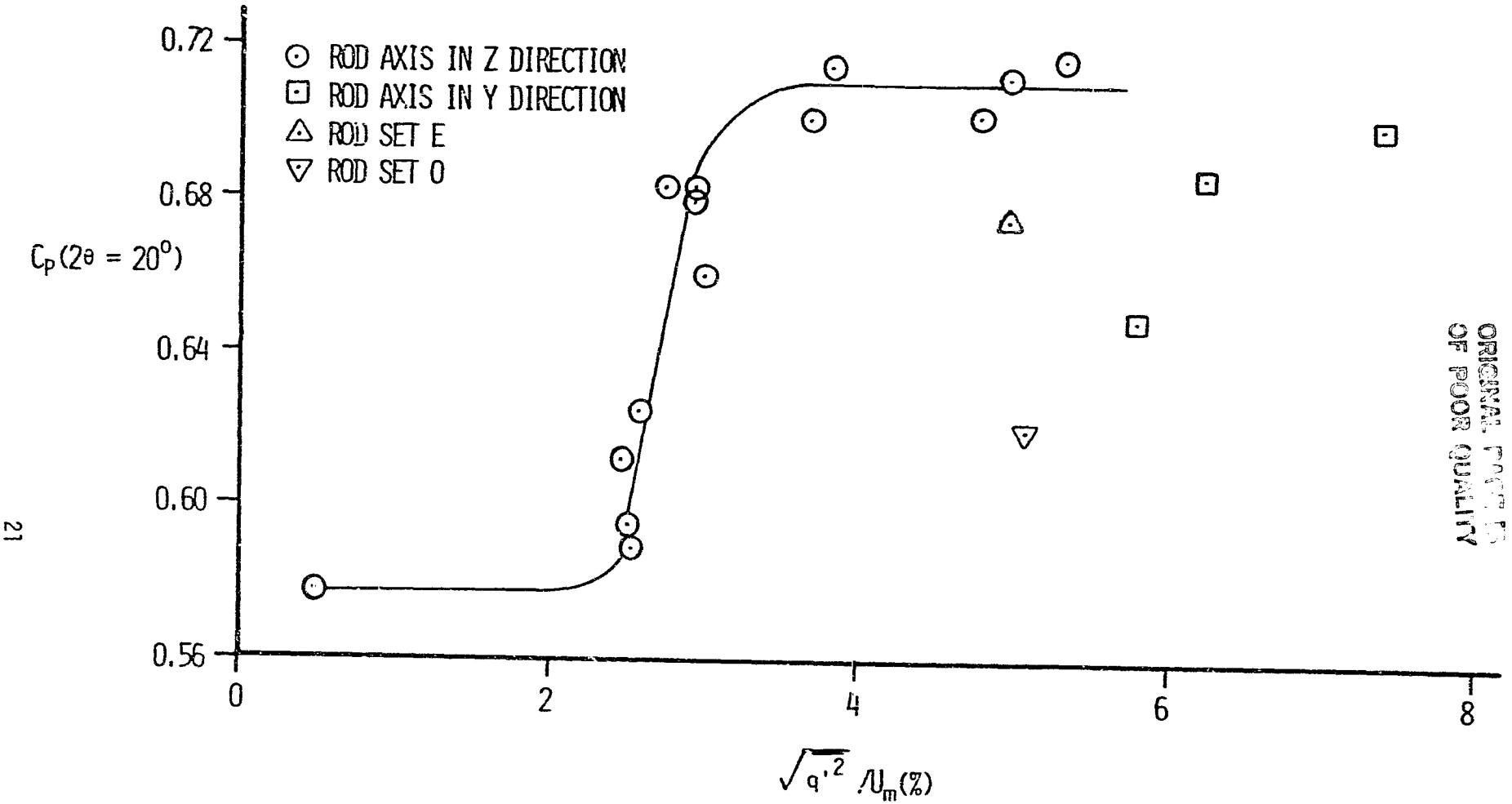

Figure 5

$C_p(2\theta = 20^o)$ vs. $\sqrt{\overline{q'^2}}/U_m$

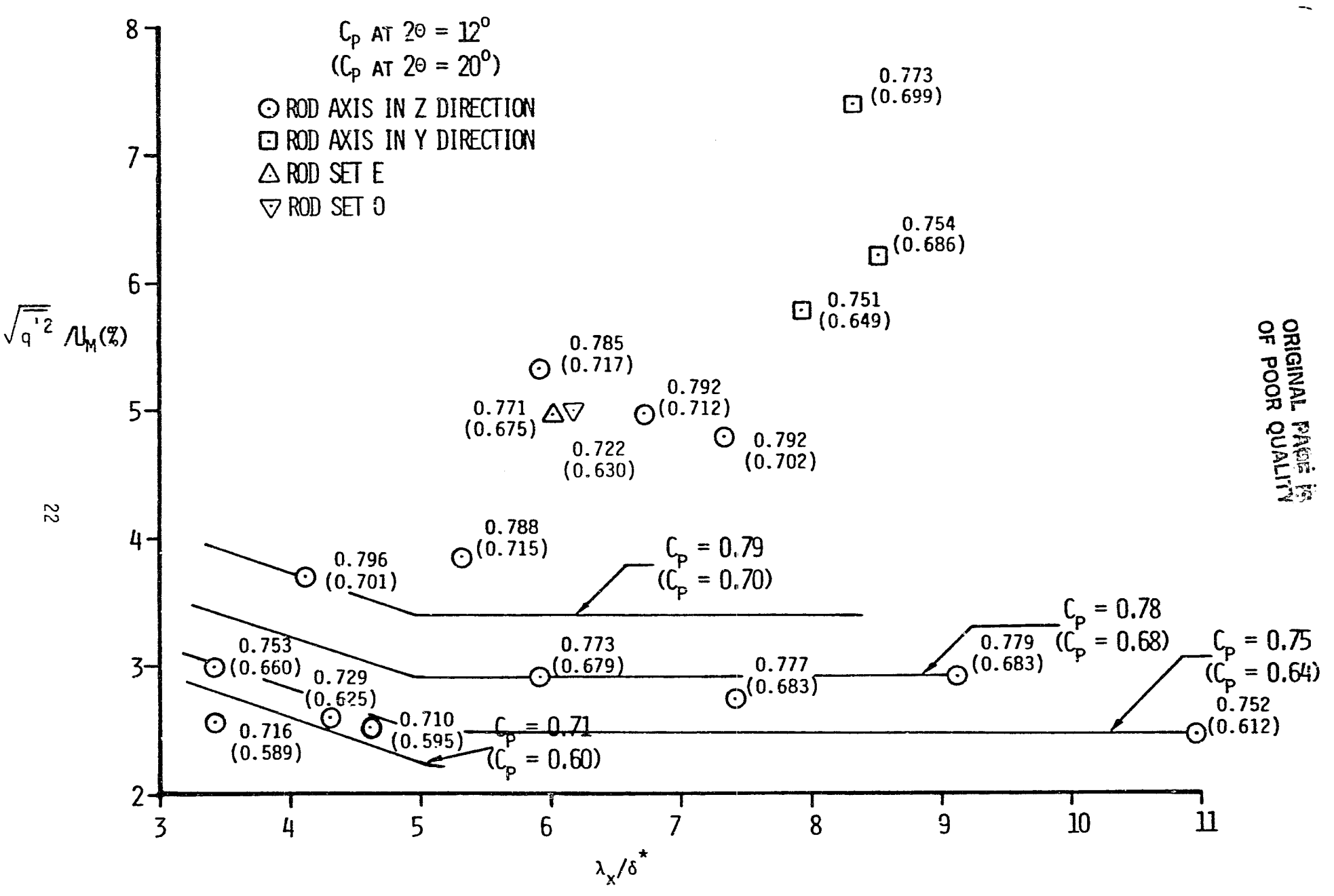

Figure 6
$\sqrt{q'^2}/U_m$ vs. λ_x/δ^* with C_p Contours

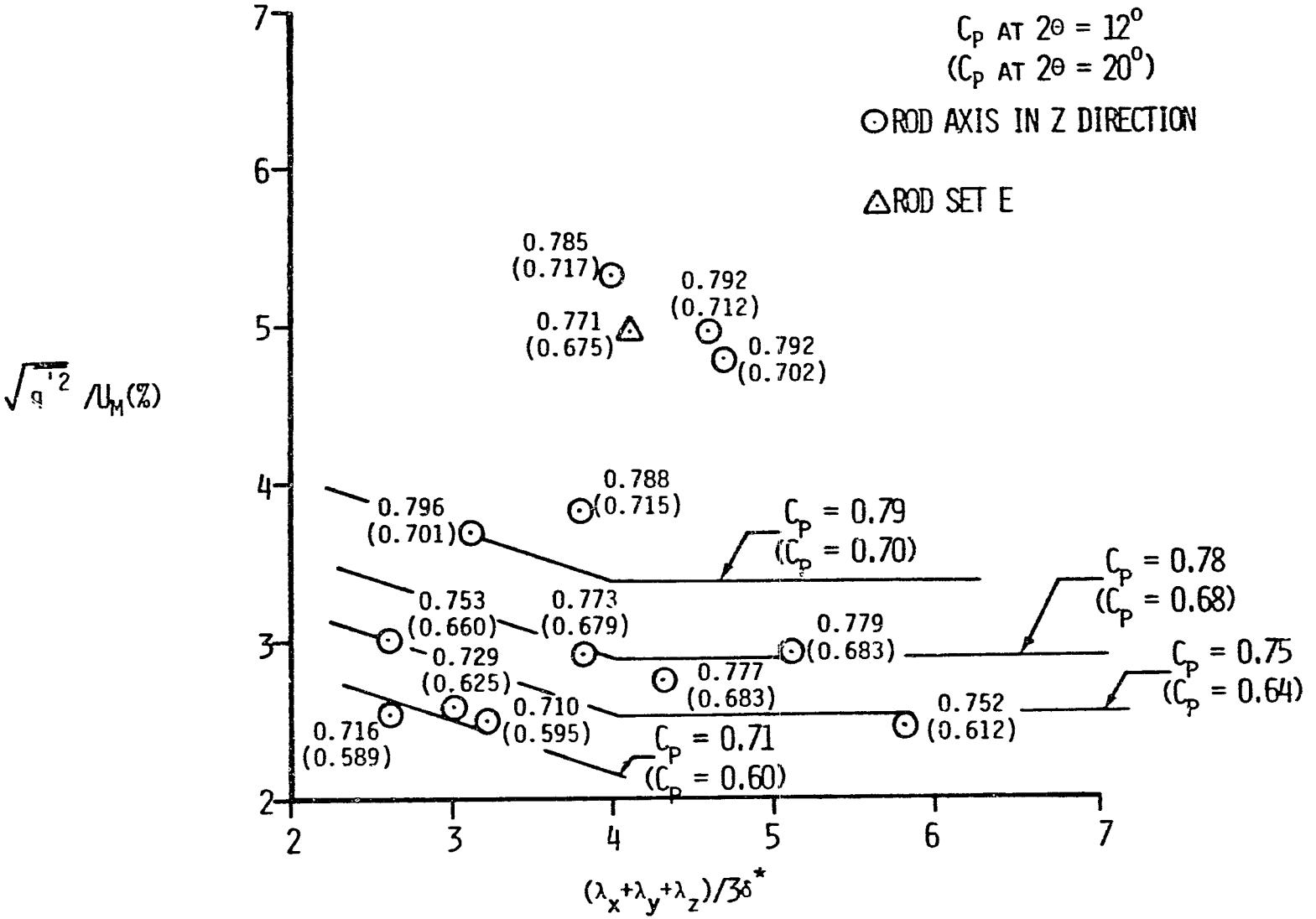

Figure 7

$\sqrt{q'^2}/U_m$ vs. $(\lambda_x + \lambda_y + \lambda_z)/3\delta^*$
with C_p Contours

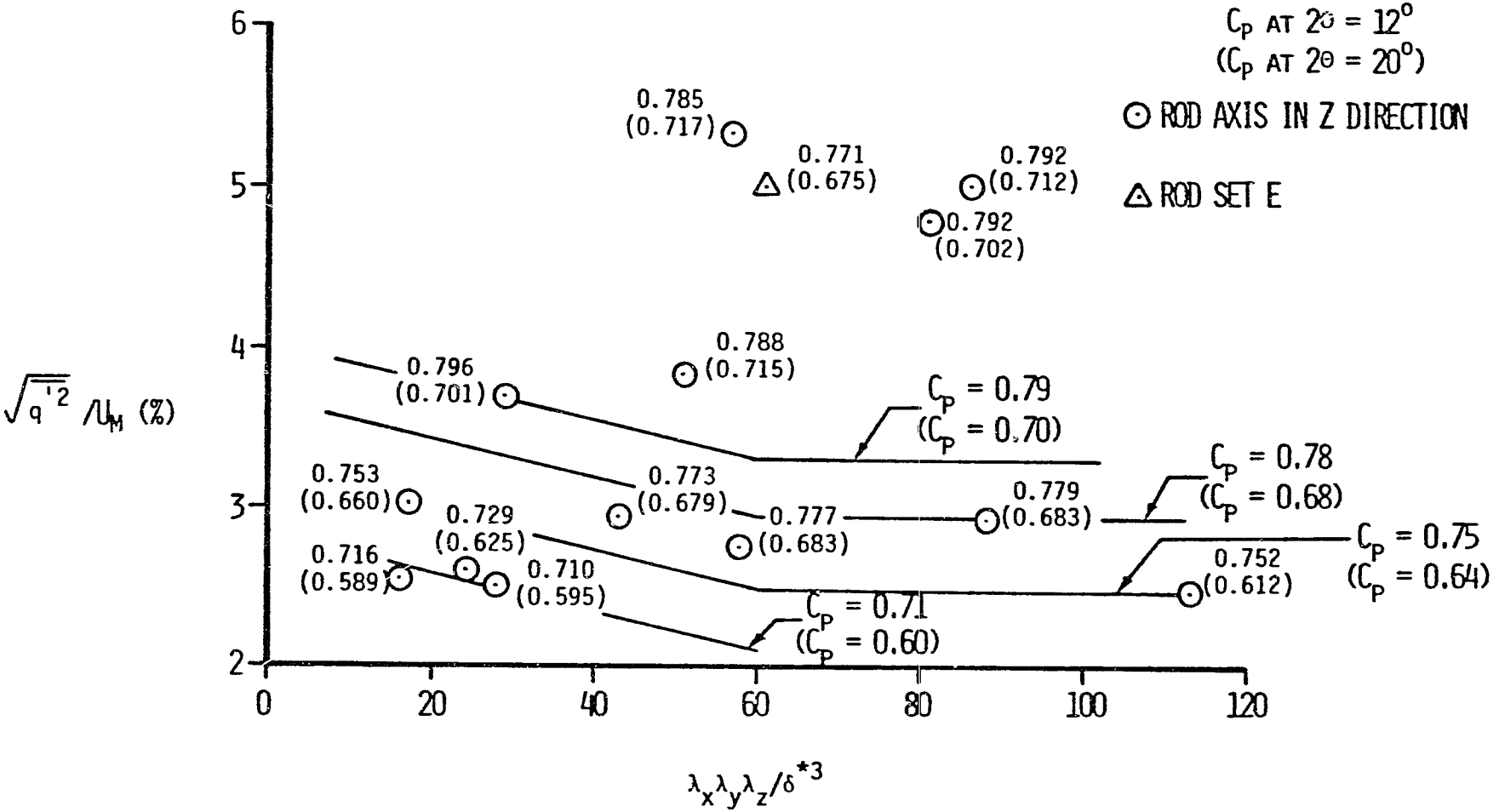

Figure 8

$\sqrt{q'^2}/U_m$ vs. $(\lambda_x\lambda_y\lambda_z)/\delta^{*3}$

with C_p Contours